

# A new look inside Planetary Nebula LoTr 5: A long-period binary with hints of a possible third component

A. Aller<sup>1\*</sup>, J. Lillo-Box<sup>2</sup>, M. Vučković<sup>1</sup>, H. Van Winckel<sup>3</sup>, D. Jones<sup>4,5</sup>,  
B. Montesinos<sup>6</sup>, M. Zorotovic<sup>1</sup>, and L. F. Miranda<sup>7</sup>

<sup>1</sup>*Instituto de Física y Astronomía, Facultad de Ciencias, Universidad de Valparaíso, Gran Bretaña 1111, Playa Ancha, Valparaíso, 2360102, Chile*

<sup>2</sup>*European Southern Observatory (ESO), Alonso de Cordova 3107, Vitacura, Casilla 19001, Santiago de Chile, Chile*

<sup>3</sup>*Instituut voor Sterrenkunde, KU Leuven, Celestijnenlaan 200D bus 2401, 3001, Leuven, Belgium*

<sup>4</sup>*Instituto de Astrofísica de Canarias, 38205 La Laguna, Tenerife, Spain*

<sup>5</sup>*Departamento de Astrofísica, Universidad de La Laguna, 38206 La Laguna, Tenerife, Spain*

<sup>6</sup>*Departamento de Astrofísica, Centro de Astrobiología (INTA-CSIC), PO Box 78, E-28691 Villanueva de la Cañada (Madrid), Spain*

<sup>7</sup>*Instituto de Astrofísica de Andalucía - CSIC, C/ Glorieta de la Astronomía s/n, E-18008 Granada, Spain*

Accepted XXX. Received YYY; in original form ZZZ

## ABSTRACT

LoTr 5 is a planetary nebula with an unusual long-period binary central star. As far as we know, the pair consists of a rapidly rotating G-type star and a hot star, which is responsible for the ionization of the nebula. The rotation period of the G-type star is 5.95 days and the orbital period of the binary is now known to be  $\sim 2700$  days, one of the longest in central star of planetary nebulae. The spectrum of the G central star shows a complex H $\alpha$  double-peaked profile which varies with very short time scales, also reported in other central stars of planetary nebulae and whose origin is still unknown. We present new radial velocity observations of the central star which allow us to confirm the orbital period for the long-period binary and discuss the possibility of a third component in the system at  $\sim 129$  days to the G star. This is complemented with the analysis of archival light curves from SuperWASP, ASAS and OMC. From the spectral fitting of the G-type star, we obtain a effective temperature of  $T_{\text{eff}} = 5410 \pm 250$  K and surface gravity of  $\log g = 2.7 \pm 0.5$ , consistent with both giant and subgiant stars. We also present a detailed analysis of the H $\alpha$  double-peaked profile and conclude that it does not present correlation with the rotation period and that the presence of an accretion disk via Roche lobe overflow is unlikely.

**Key words:** planetary nebulae: individual: LoTr 5 – binaries: general – techniques: radial velocities – techniques: photometric – stars: activity

## 1 SAGA OF LOTR 5

The planetary nebula (PN) LoTr 5 ( $\alpha_{(2000.0)} = 12^{\text{h}} 55^{\text{m}} 33^{\text{s}}.7$ ,  $\delta_{(2000.0)} = +25^{\circ} 53' 30''$ ; see Figure 1) was discovered by Longmore & Tritton (1980). It is the highest Galactic latitude PN in our Galaxy ( $b = +88^{\circ}.5$ ) and belongs to the so-called Abell 35-type<sup>1</sup> group of PNe (Bond et al. 1993). The PNe in this group are known to host a binary central star comprising a rapidly rotating giant or subgiant star plus a hot progenitor responsible for the ionization of the nebula. These objects

have some resemblance to other long-period binaries as, e.g., the high-galactic-latitude HD 128220 (see Heber 2016, and references therein) in which possible associated PNe would have already dissipated. The optical spectrum of HD 112313, the central star of LoTr 5 (also named IN Comae), is completely dominated by a rapidly rotating G-type star. The evolutionary status of this star is uncertain and both giant and subgiant solutions have been suggested in the literature (Strassmeier et al. 1997). The hot component was firstly found by Feibelman & Kaler (1983) by analyzing ultraviolet spectra, in which the flux peak showed an extremely hot (over 100 000 K) component. Since then, searches for long- and short-period variability have been persistently done, culminating in the recent detection of a long orbital period binary (Van Winckel et al. 2014; Jones et al. 2017).

Photometric variability in HD 112313 was firstly found

\* E-mail: alba.aller@ifa.uv.cl

<sup>1</sup> As already discussed in Tyndall et al. (2013), we consider that the Abell 35-type PNe designation is not longer appropriate, since Abell 35 is most likely a Strömgren zone in the ambient interstellar medium (Frew 2008) and not a true PN.

by Schnell & Purgathofer (1983), who reported four different periods between 0.35 and 1.2 days, although they stated that the 1.2-day period was the most probable. Later on, Noskova (1989) detected the 5.9 days period, which was independently found by H. E. Bond in 1988 (see Bond & Livio 1990). This 5.9 days period was also confirmed in the subsequent years by Kuczawska & Mikolajewski (1993), Jasniewicz et al. (1996), and Strassmeier et al. (1997), who interpret this period as the rotational period of the G-type star and the 1.2 days period as an alias of the true period. This is still assumed today.

Parallel to these works, radial velocity variations were also further discussed. Acker et al. (1985) were the first to detect radial velocity variations in HD 112313 and they derived a probable (but questionable due to imprecision of the observations) period of 0.35 days. Two years later, Jasniewicz et al. (1987), with CORAVEL high-resolution spectra, proposed a triple scenario for the system, consisting of an inner close-binary of 1.99 days orbital period (with two similar components), and an outer, third companion (the hot sdO star) with  $\sim 540$  days orbital period. Malasan et al. (1991) also concluded the triple scenario, but with a different configuration: a 1.75 days period for the inner system and 2000 days for the outer one, being doubtful whether the sdO belongs to the inner or outer orbit. Jasniewicz et al. (1994), apart from photometric variations, also detected radial velocity variations although no stable period was found due to the poor quality of the spectra. Strassmeier et al. (1997) also obtained radial velocity variations but they concluded that they were due to the influence of starspots. The periodicity of several years was confirmed by Van Winckel et al. (2014), although they did not cover the full radial velocity curve. After all of these efforts, the orbital period has been recently unveiled by Jones et al. (2017), being one of the longest period measured in a central star of a PN ( $\sim 2700$  days; see Jones & Boffin 2017, for comparison with the period distribution of all the binary central stars). Ciardullo et al. (1999) obtained high-resolution images of the nucleus of LoTr 5 with the Hubble Space Telescope but failed to resolve the binary, although this might be due to the very small angular separation of the binary and/or to the faintness of the hot star.

Even though the orbit has already fully covered, there is still no clear scenario for this peculiar system. From high-resolution, long-slit spectra of the nebula, Graham et al. (2004) proposed a bipolar model for LoTr 5, in which the bipolar axis is tilted by  $\sim 17^\circ$  to the line of sight. However, that inclination is at odds with the mass function derived by Jones et al. (2017), who proposed several explanations to solve the mass problem. One possibility is that the inclination of the nebula is incorrect. This solution seems to be the most probable since, a small change in the inclination would resolve the mass problem: for example, for inclinations  $> 23^\circ$ , the mass of the primary would be less than the Chandrasekhar limit ( $1.4 M_\odot$ ). Another possibility is that the bipolar axis of the nebula is not perpendicular to the orbital plane of the binary.

It is also worth to mention that LoTr 5 is one of the PNe with a 'Barium star' central star (Miszalski et al. 2013; Tyndall et al. 2013). Barium stars are characterized by a strong enhancement of the barium abundance and other s-process elements such as Sr and Y (Bidelman & Keenan

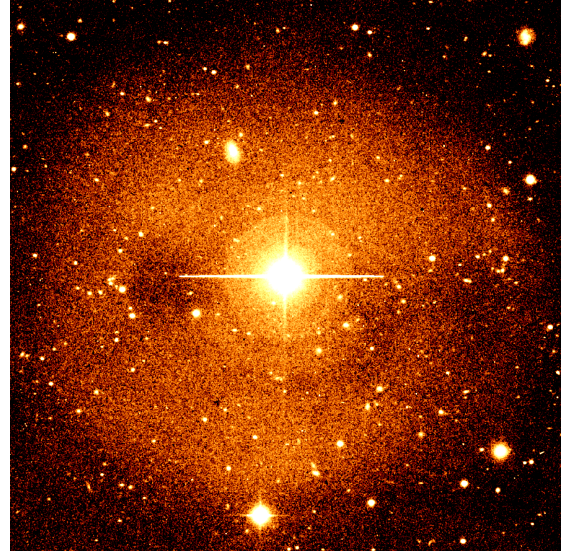


**Figure 1.** Image of LoTr 5 taken with the Isaac Newton Telescope's Wide Field Camera in the  $H\alpha$  filter. The size of the field is  $9' \times 9'$ . North is up and East is left.

1951), as already showed by Thevenin & Jasniewicz (1997) in their spectral analysis of the G-star of LoTr 5. This could be consequence of the contamination of the photosphere by the transfer material of s-process-overabundant material from the former AGB star (which is now the central star). This contamination process is thought to occur via wind-accretion and not through a common envelope evolution (Boffin & Jorissen 1988; Jeffries & Stevens 1996), which is in agreement with the long orbital period derived for the system (see Jones et al. 2017).

Another remarkable aspect of HD 112313 is its  $H\alpha$  double-peaked profile that varies with very short time scales. This profile was firstly reported by Jasniewicz et al. (1994) and the origin is still unknown. The main causes proposed to explain it have been the presence of an accretion disc, the chromospheric activity of the G star, and/or stellar winds. Regarding the last point, Modigliani et al. (1993) reported a fast wind speed of  $3300 \text{ km s}^{-1}$  from the IUE spectra, although the evidence for a such wind was questioned by Montez et al. (2010). Finally, HD 112313 was also confirmed as an X-rays emitter by Apparao et al. (1992) with the EXOSAT satellite. Later, Montez et al. (2010) detected point source X-ray emission of HD 112313 with XMM and CXO spectra, stating that the most likely scenario is the presence of coronal activity associated with the G-type star.

In this work, we revisit this complex system and present new radial velocity data of HD 112313, which allow us to confirm the orbital period for the long-period binary and examine the possibility of a third component in the system close to the G-type star. These new data are complemented with the analysis of the archival light curves from SuperWasp, OMC and ASAS, that have not been published to date. In addition, a detailed analysis of the  $H\alpha$  double-peaked profile is presented as well as the analysis of the IUE spectra available for this object.

## 2 OBSERVATIONS AND DATA REDUCTION

### 2.1 High-resolution, optical spectroscopy

We used high-resolution spectra of HD 112313 from both archival and new observations obtained from different facilities.

We performed dedicated observations of this target using the Calar Alto Fiber-fed Echelle spectrograph (CAFE, [Aceituno et al. 2013](#)) mounted on the 2.2-m telescope at Calar Alto Observatory (Almería, Spain). CAFE covers the 4000–9500 Å spectral range with an average spectral resolution of  $\lambda/\Delta\lambda = 63\,000$ . We acquired 6 high-resolution spectra on 2012 May 18–22. The exposure times were fixed to 900 s, with the signal-to-noise ratio ranging from 20 to 80 depending on the weather and seeing conditions, and one noisy spectra having  $S/N < 10$ . The spectra were reduced with observatory’s pipeline described in [Aceituno et al. \(2013\)](#), which performs the standard routines for echelle spectroscopy: bias subtraction, order tracing, flat field correction, and wavelength calibration based on ThAr lamp frames obtained right after each science frame.

The radial velocity was extracted from the individual spectra by cross-correlating them against a G2V binary mask ([Baranne et al. 1996](#)) specially designed for the CAFE data and already used in planet-detection studies (e.g., [Lillo-Box et al. 2015](#)). Given the fast-rotating nature of the G-type star ( $v \sin i \sim 66.2 \pm 0.7 \text{ km s}^{-1}$ , [Van Winckel et al. 2014](#)), the cross-correlation function (CCF) was fitted to a rotational profile defined by [Gray \(2005\)](#) and already used in planet-related studies like [Santerne et al. \(2012\)](#)

$$G(v) = \frac{2(1 - \epsilon) \sqrt{1 - (v/v_L)^2} + 0.5\pi\epsilon [1 - (v/v_L)^2]}{\pi v_L (1 - \epsilon/3)} \quad (1)$$

where  $v_L = v \sin i$  and  $\epsilon$  is a limb-darkening coefficient, that we fix to  $\epsilon = 0.3$  for the CCF modeling purposes in this paper as done in [Santerne et al. \(2012\)](#). We note that this coefficient is not critical since radial velocities just change within the uncertainties for different values of  $\epsilon$ . This profile was convolved with the instrumental profile of CAFE, that we assume to be a Gaussian with a FWHM = 8.3  $\text{km s}^{-1}$ . The results of the CCF fitting are presented in Figure 2 and the radial velocities with their corresponding uncertainties are summarized in Table 1. The CAFE radial velocity data taken in the same night have been combined to increase the precision.

In addition, we retrieved the high-resolution echelle spectra of HD 112313 from the archive of the ELODIE<sup>2</sup> ([Moutaka et al. 2004](#)) spectrograph at the Observatoire de Haute-Provence 1.93-m telescope. The spectra cover a spectral range of 4000–6800 Å with a resolution of  $R = 42\,000$ . For HD 112313, the ELODIE archive provides three epochs: two with exposure times of 3600 s and S/N of 128 and 76, respectively, taken in 1998 March 7–8; and another with 900 s and a S/N of 23, taken in 2003 March 11. The ELODIE archive also provides the radial velocity of each spectrum calculated by cross-correlating it with numerical masks of F0 or K0 spectral types. However, these radial velocities are obtained by fitting the CCF with a Gaussian profile, which is

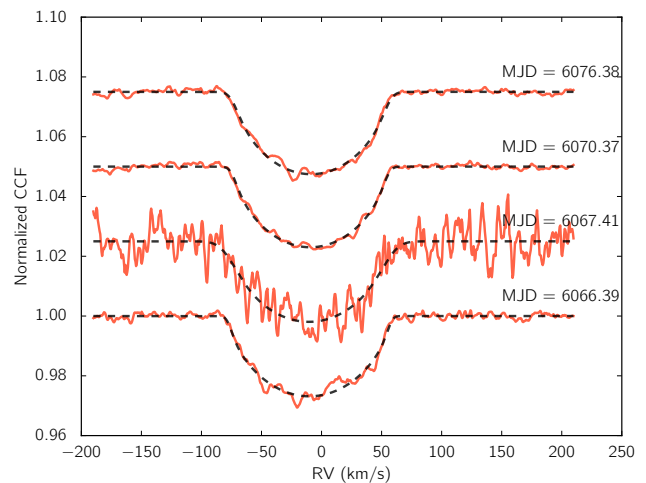


**Figure 2.** Cross-correlation functions of the CAFE spectra (solid red line) and their fitted profiles (dashed black line). The modified julian date (MJD) is indicated in each plot as JD-2450000.

**Table 1.** Radial velocity measurements from CAFE and ELODIE used in the analysis.

Julian date	RV ( $\text{km s}^{-1}$ )	Instrument
2450879.090356	$-14.80 \pm 0.28$	ELODIE
2450880.0942862	$-15.64 \pm 0.33$	ELODIE
2452709.9643882	$-9.20 \pm 0.45$	ELODIE
2456066.39055	$-10.062 \pm 0.17$	CAFE
2456067.40529	$-10.52 \pm 0.75$	CAFE
2456070.37146	$-9.45 \pm 0.11$	CAFE
2456076.37568	$-8.75 \pm 0.13$	CAFE

not suitable in this case due to the broad CCF given the fast rotation of the star. For that reason, we have re-calculated the radial velocity values by using the G2V binary mask and fitting the CCF with the same rotational profile used in the CAFE data. The radial velocities with their corresponding uncertainties are shown in Table 1.

Finally, we have also used the data published in [Jones et al. \(2017\)](#) for this object, taken with the HERMES spectrograph ([Raskin et al. 2011](#)) on the 1.2m Mercator telescope, as part of a large radial-velocity monitoring programme. The data consist of 210 radial velocity measurements with a very high precision that have been critical to confirm the long-period binary star. The radial velocities from HERMES can be found in [Jones et al. \(2017\)](#).

### 2.2 Archival photometry

We retrieved the photometric time series for HD 112313 from the surveys SuperWASP (Wide Angle Search for Planets; [Pollacco et al. 2006](#)), ASAS-3 (All Sky Automated Survey) Photometric V-band Catalogue ([Pojmanski 1997](#)) and OMC (Integral’s Optical Monitoring Camera; [Mas-Hesse et al. 2003](#)).

The SuperWASP monitoring covers 116 days with 5323 data points taken with a broad band passband from 400 to 700 nm. We retrieved the data from the SuperWASP

<sup>2</sup> <http://atlas.obs-hp.fr/elodie/>



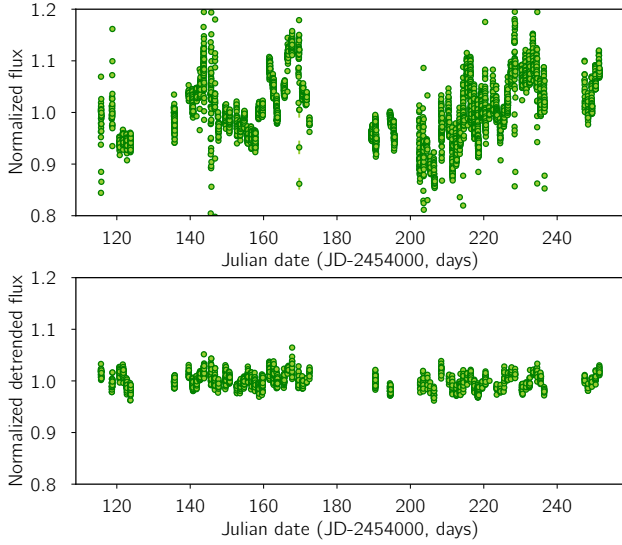


**Figure 3.** SuperWASP light curve. Top: undetrended flux from the superWASP archive. Bottom: Detrended flux by using the close-by star HD 112299 as reference.

Public Archive<sup>3</sup>. Given the large instrumental imprints in the flux, we also retrieved the photometric data from a star close to the target in order to remove these drifts in a precise manner. We then performed differential photometry by using HD 112299 as a reference star. The original and detrended light curves are shown in Fig. 3. The OMC data, taken in the Johnson V-band, were retrieved from the OMC Archive<sup>4</sup> and provide a time span of the observations of 3646 days with 2745 data points. Here we have cleaned the light curve following the criteria in Alfonso-Garzón et al. (2012) with the aim of improving the quality of the data. In the case of the ASAS data, retrieved from the ASAS All Star Catalogue<sup>5</sup>, we only have 272 data points in 2370 days time span. ASAS provides photometry with 5 different apertures. For stars with magnitudes brighter than 9 (as it is the case of HD 112313), it is recommended to use the one with the widest aperture (*MAG4*<sup>6</sup>).

The Optical Monitoring Camera (OMC) on board the high-energy INTEGRAL satellite provides photometry in the Johnson V-band within a 5 by 5 degree field of view.

### 2.3 Low resolution ultraviolet spectra

We have retrieved all the IUE (International Ultraviolet Explorer; Kondo et al. 1989) spectra available in the IUE Newly Extracted Spectra (INES<sup>7</sup>) System for HD 112313. INES provides spectra already calibrated in physical units.

We have retrieved the available low-dispersion ( $\sim 6 \text{ \AA}$ ) IUE SWP (short wavelength) and LWP (long wavelength) spectra, which were obtained from 1982 to 1990. The SWP

**Table 2.** Summary of the IUE observations available in the INES database for HD 112313.

Spectrum	Exp (s)	Date
SWP16896	1200	1982-05-05
SWP16897	1200	1982-05-05
LWR13173	1200	1982-05-05
SWP17236	600	1982-06-16
LWR13502	600	1982-06-16
LWR15882	2100	1983-05-05
SWP19909	300	1983-05-05
LWR15883	300	1983-05-05
LWR15884	5100	1983-05-05
SWP35635	480	1989-02-28
SWP35643	900	1989-03-01
SWP35688	1200	1989-03-06
LWP15137	1200	1989-03-06
SWP35709	1200	1989-03-08
LWP17022	1080	1989-12-28
SWP37912	900	1989-12-28
SWP37912	1200	1989-12-28
LWP17023	480	1989-12-28
LWP17042	720	1989-12-30
SWP37923	900	1989-12-30
LWP17063	600	1990-01-01
LWP17063	600	1990-01-01
SWP37932	900	1990-01-01
SWP37936	900	1990-01-02
LWP17070	720	1990-01-02
LWP17070	600	1990-01-02
SWP37937	20280	1990-01-02
SWP38776	20400	1990-05-12

and LWP spectra cover the ranges 1150-1975  $\text{\AA}$  and 1910-3300  $\text{\AA}$ , respectively. In total, 28 SWP and LWP spectra are available. They are listed in Table 2, with the exposure times and the date of the observations. We discarded the spectra with many bad pixels and/or those that appear to be saturated.

## 3 RESULTS

### 3.1 Spectral fitting of the G-type secondary

The exact spectral type and evolutionary status of the G-type companion is uncertain, with both giant and subgiant solutions being possible (Strassmeier et al. 1997). In order to attempt to resolve this ambiguity, we fit the high signal-to-noise HERMES spectra using the spectral synthesis and modelling tool iSpec (Blanco-Cuaresma et al. 2014). MARCS model atmospheres (Gustafsson et al. 2008) were used to produce synthetic spectra using the SPECTRUM spectral synthesis code (Gray & Corbally 1994), which were then iteratively fit to the observed spectrum following the chi-squared minimisation routine outlined in (Blanco-Cuaresma et al. 2014). The effective temperature, surface gravity and metallicity were allowed to vary, while the rotational broadening was fixed to a value of  $v \sin i = 66.2 \text{ km s}^{-1}$  as determined by Van Winckel et al. (2014). The resulting effective temperature,  $T_{\text{eff}} = 5410 \pm 250 \text{ K}$ , and surface gravity,  $\log g = 2.7 \pm 0.5$ , are consistent with both giant and subgiant possible companions, while the low derived metallicity,  $[\text{Fe}/\text{H}]$

<sup>3</sup> <http://wasp.cerit-sc.cz/form>

<sup>4</sup> [https://sdc.cab.inta-csic.es/omc/secure/form\\_busqueda.jsp](https://sdc.cab.inta-csic.es/omc/secure/form_busqueda.jsp)

<sup>5</sup> <http://www.astrow.edu.pl/asas/?page=aasc&catsrc=asas3>

<sup>6</sup> <http://www.astrow.edu.pl/asas/explanations.html>

<sup>7</sup> <http://sdc.cab.inta-csic.es/ines/>

**Table 3.** Results from the light curve analysis of the three datasets.

Parameter	SuperWASP	ASAS	OMC
Period (days)	$5.9508 \pm 0.0006$	$5.9670 \pm 0.0014$	$5.9702 \pm 0.0002$
$\phi_0$ (days)	$2452652.01 \pm 0.16$	$2452652.30 \pm 0.21$	$2452651.951 \pm 0.043$
Amplitud (mmag)	$12.93 \pm 0.52$	$20.2 \pm 2.9$	$18.12 \pm 0.41$
Date interval	2007 Jan – 2007 May	2003 June – July 2009	2003 Jan – 2013 Jan
Number of data points	5323	242	2745

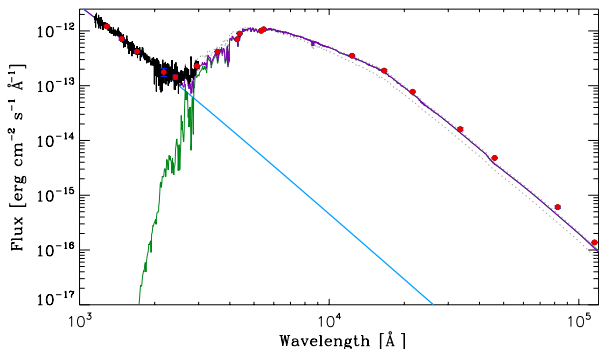


**Figure 4.** Spectral energy distribution (SED) of HD 112313 constructed with VOSA. One IUE spectrum is also included. The blue line corresponds to a blackbody with  $T_{\text{eff}} = 150000$  K. The green line corresponds to a Kurucz model with  $T_{\text{eff}} = 5410$  K and  $\log g = 2.70$ . In purple is the composite model. The dotted grey lines represent the models with  $T_{\text{eff}} = 5160$  K and  $T_{\text{eff}} = 5660$  K, corresponding to the 1-sigma boundaries of the estimated effective temperature of LoTr 5.

$= -0.1 \pm 0.1$  (assuming solar abundances from [Grevesse et al. 2007](#)), is consistent with the high galactic latitude of LoTr 5.

### 3.2 Spectral energy distribution

We have analyzed the spectral energy distribution (SED) of HD 112313 by using the Virtual Observatory SED Analyzer (VOSA, [Bayo et al. 2008](#)), in order to search for infrared excess. Figure 4 presents the SED with the magnitudes from Tycho, UBV from Mermilliod 1991, 2MASS Point Source Catalog, and WISE archive. One IUE spectrum has been superimposed in the SED. In green, we have plotted a Kurucz model for the G-type star with  $T_{\text{eff}} = 5410$  K and  $\log g = 2.70$  and in blue a blackbody with  $T_{\text{eff}} = 150000$  K, to account for the hot star. The blackbody has not been reddened since the high Galactic latitude of LoTr 5 makes the extinction practically negligible. The planetary nebula is very faint so, apparently, there is not contamination from the nebula either. As can be seen in Fig. 4, no significant infrared excess can be identified, which would point out that there is no evidence for additional components (e.g., a third companion and/or an accretion disk) in the system. We will discuss in detail these possibilities below.

### 3.3 Archival light curves analysis

In Fig. 5, we show the Lomb-Scargle periodograms of the three photometric datasets. In the case of superWASP and ASAS, we find a significant peak at  $P \sim 5.95$  days (assumed to be the rotation period of the (sub)giant star, see Sect. 1). We can model this signal with a simple sinusoid to estimate the period and amplitude of the variations independently in each dataset. We left the period to vary freely between 0 and 10 days in all cases and found:  $P_{\text{WASP}} = 5.95092 \pm 0.00062$  days,  $P_{\text{ASAS}} = 5.9409 \pm 0.0021$  days,  $P_{\text{OMC}} = 5.94579 \pm 0.00012$  days. Fig. 6 shows the phase-folded light curves of the three datasets with these periods. The corresponding semi-amplitudes are  $A_{\text{WASP}} = 12.93 \pm 0.52$  mmag,  $A_{\text{ASAS}} = 20.2 \pm 2.9$  mmag,  $A_{\text{OMC}} = 18.12 \pm 0.41$  mmag. These results, together with the date range of the data, are summarized in Table 3. The amplitude clearly varies from one lightcurve to each others. This might be due to the different timespan of the datasets covering different time ranges of the stellar cycle (i.e., different amount of star spots). In the case of SuperWASP, the data were taken in a short time span (only four months), so the stellar spots are steady along this time. On contrary, in the case of ASAS and OMC, where the data are spread over years, the amplitude due to star sports is diluted because we are probably mixing periods of stellar maxima and stellar minima.

If we now remove this signal from the SuperWASP dataset (the most precise one) and calculate the periodogram of the residuals, other prominent (although non-significant) peaks appear (see Fig. 7, top panel). In particular, we want to highlight the peak at  $\sim 129$  days. This is relevant because it also appears in the radial velocity analysis (see Sect. 3.4.3). The phase-folded light curve with that period is shown in Fig. 7, bottom panel. The origin of this peak will be discussed in detail in Sect. 3.4 together with the  $\sim 5.95$  days periodicity.

### 3.4 Radial velocity analysis

#### 3.4.1 The long-term companion

In Figure 8, we show the radial velocity data described in Sect. 2.1, covering 20 years time span and including ELODIE, HERMES and CAFE observations. They clearly show the long-term variations found in [Jones et al. \(2017\)](#), corresponding to a  $\sim 7.4$ -years period eccentric companion to the fast rotating G-type star. For the first time, we report the coverage of two cycles in the orbit, with values in perfect agreement with the scenario proposed in [Jones et al. \(2017\)](#). Given the new data, the Lomb-Scargle periodogram of the radial velocities shows a clear peak at  $\sim 2700$  days. We have modelled these radial velocity data by using six free

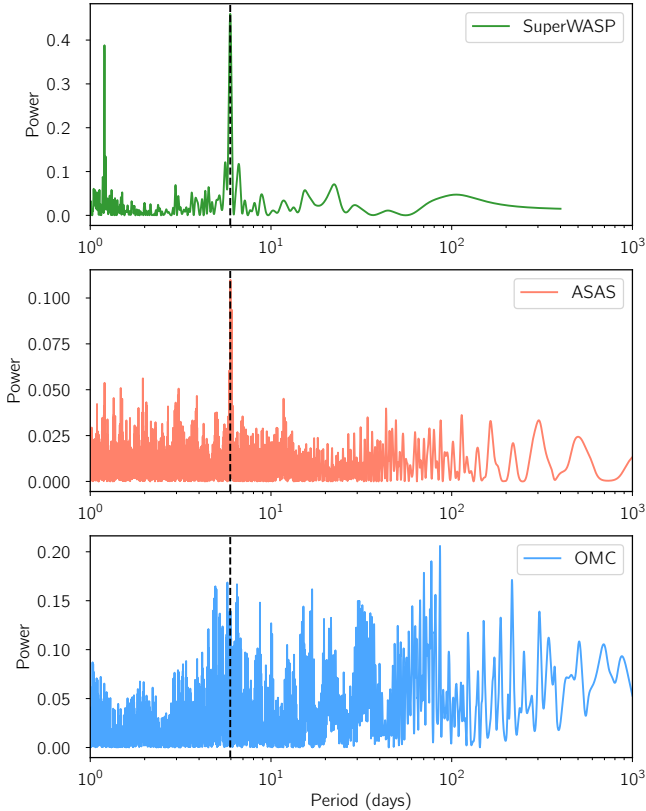


**Figure 5.** Lomb-Scargle periodogram of the light curves provided by the three datasets used. The dashed vertical line indicates the  $\sim 5.95$  days period.

parameters to account for the orbital and physical properties of the long-period companion: period ( $P$ ), time of periastron passage ( $T_0$ ), systemic velocity of the system ( $V_{\text{sys}}$ ), radial velocity semi-amplitude ( $K$ ), eccentricity ( $e$ ) and argument of the periastron ( $\omega$ ). Added to this, we included a radial velocity offset for each instrument pair ( $N_{\text{inst}}-1$  additional parameters) and a jitter term for each instrument ( $N_{\text{inst}}$  additional parameters) to account for possible white noise mainly due to underestimated uncertainties or unaccounted instrumental effects. So, in total, we fitted for 11 parameters.

We used the implementation of Goodman & Weare’s affine invariant Markov chain Monte Carlo (MCMC) ensemble sampler *emcee*<sup>8</sup>, developed by Foreman-Mackey et al. (2013) to sample the posterior probability distribution of each of those parameters. We set uniform priors to all parameters in the ranges stated in Table A1 and used 50 walkers with 5000 steps each. The posteriors are then computed by combining the latter half of all chains to avoid any possible dependency with the initial parameters. The chains converged quickly and show no clear correlations between the parameters. In Table 4 we show the median and 68.7% confidence intervals for the different parameters.

The median solution provides a period of  $2689 \pm 52$  days

<sup>8</sup> See <http://dan.iel.fm/emcee/current/> for further documentation.

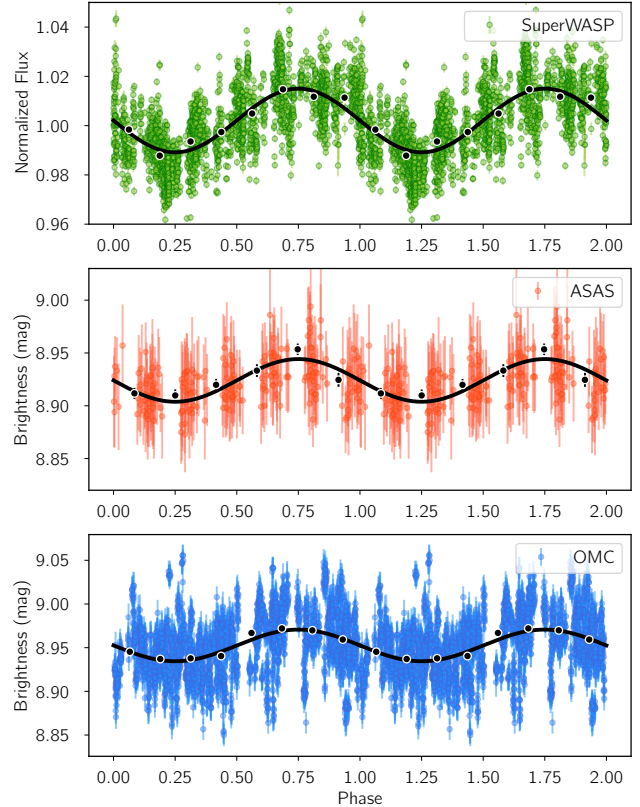


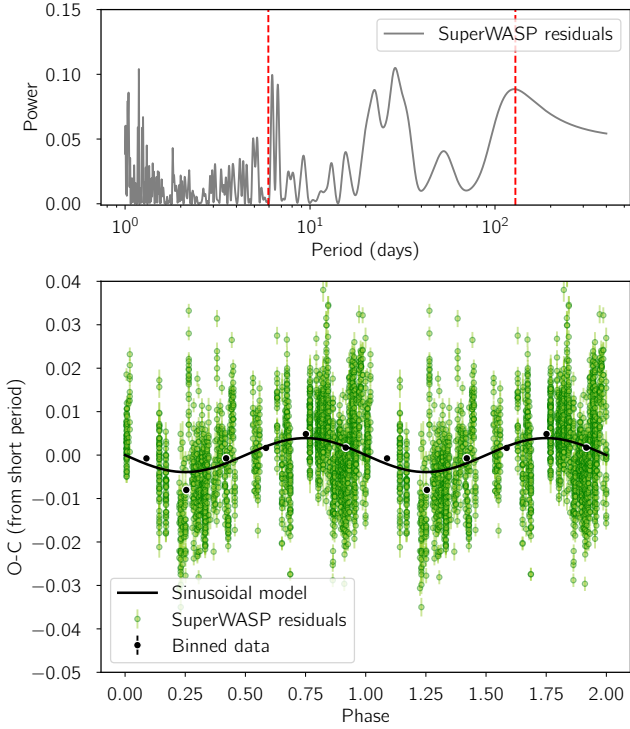
**Figure 6.** Phase-folded light curves with the best fitted period for each of the three datasets, namely SuperWASP (top), ASAS (middle), and OMC (bottom). The black line shows the fitted sinusoidal model and the black circles represent the binned data.

and an eccentricity of  $0.249 \pm 0.018$ , in agreement with those derived by Jones et al. (2017). These values and their corresponding confidence intervals are listed in Table 4. Assuming a mass for the (sub)giant star of  $1.1 M_{\odot}$ , we obtain a minimum mass for the companion of  $m_2 \sin i = 0.499 M_{\odot}$ . If we assume that the orbital plane of the binary is coplanar with the waist of the nebula, then the inclination angle of the system is  $i = 17^{\circ}$  (see Graham et al. 2004) and the absolute mass for the companion would be  $1.5 M_{\odot}$ . This mass is incompatible with a white dwarf-like star. However, this is not very conclusive, since the orbital plane might not be coplanar with the waist of the nebula and/or the inclination of the system might be different than that derived from the model by Graham et al. (2004). For example, assuming that the inclination angle of the system is  $i \sim 45^{\circ}$  (as proposed by Strassmeier et al. (1997)), a mass for the companion of  $\sim 0.7 M_{\odot}$  is obtained, which is clearly in the range of the central stars of PNe. Also, with smaller inclinations ( $> 23^{\circ}$ ) we obtain a white dwarf mass below the Chandrasekhar limit ( $1.4 M_{\odot}$ ).

However, if we assume coplanarity of the long-period orbit and the waist of the nebula, the mass of this second object would be outside of the typical masses for a PN progenitor. Consequently, as stated by Jones et al. (2017), either this long-period companion is not coplanar with the waist of the nebula, or the inclination of the waist is much larger

**Table 4.** Best fit from the radial velocity analysis.

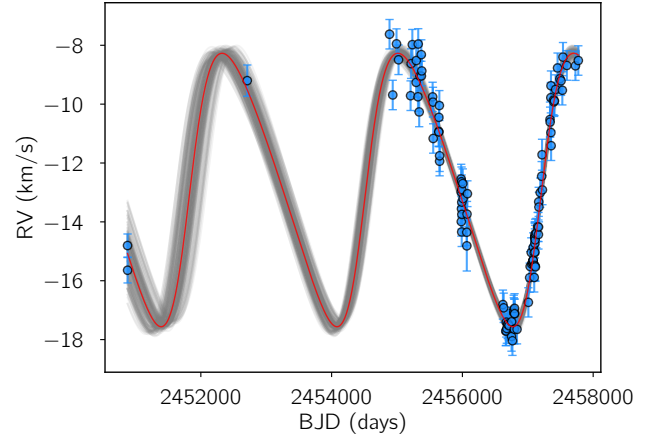
Parameter	Long-period	5.95d	~129d (circ)	~129d (ecc)
$V_{\text{sys}}$ (km s $^{-1}$ )	$-8.53 \pm 0.37$	-	$-0.009 \pm 0.090$	$-0.020 \pm 0.080$
$P$ (days)	$2689 \pm 52$	$5.96675 \pm 0.00051$	$128.9^{+6.1}_{-5.7}$	$129.8 \pm 1.6$
$T_0$ (days)	$2455944 \pm 25$	-	-	$2454976^{+50}_{-8}$
$K$ (km s $^{-1}$ )	$4.630 \pm 0.084$	$0.609 \pm 0.028$	$0.089^{+0.107}_{-0.079}$	$0.279^{+0.028}_{-0.133}$
$e$	$0.249 \pm 0.018$	-	0.0	$0.60^{+0.17}_{-0.31}$
$w$ ( $^{\circ}$ )	$259.9 \pm 4.8$	-	-	$-26^{+33}_{-31}$


**Figure 7.** Top: Periodogram of the residuals of the superWASP data after removing the  $\sim 5.95$  days signal. The  $\sim 129$  days peak is also marked with a vertical dashed line. Bottom: Light curve residuals after removing the  $\sim 5.95$  days signal and phase-folded with the 129 days periodicity

than the reported  $17^{\circ}$ , or the PN progenitor is blended in a close binary system forming a hierarchical triple. Thus, in the following section we further explore the radial velocity residuals to look for additional bodies/periodicities in the system.

### 3.4.2 The $\sim 5.9$ days period

In Figure 9, we show the Lomb-Scargle periodogram of the residuals of the radial velocity data from the long-term companion analysis. For this analysis, we have used the data from Jones et al. (2017) with  $\text{JD} \geq 2456700$ , since they have a lower dispersion in comparison with the previous data. The strongest peak corresponds to  $P \sim 5.95$  days, previously identified in our light curve analysis. This periodicity could be either explained as stellar rotation-induced activity signals (as previously assumed) or due to a third guest in the


**Figure 8.** Radial velocity of LoTr 5 in a 20 years time span covering two orbits of the long-period companion. The red line represents the median model from the posterior distribution of the fitted parameters (see text for details) and the gray lines represent a random subsample of models within the 68.7% confidence interval.

system, i.e., a low-mass short-period companion to the fast rotating G-type star. We first investigate this latter scenario (although we note that this scenario would make worse the problem with the mass of the outer white dwarf) by fitting a circular Keplerian orbit to the radial velocity after removing the long-period signal. The results of this analysis are provided in the third column of Table 4. As we show, the period perfectly matches the significant periodicity found in the light curves. The amplitude of this assumed Keplerian orbit would be of the order of 600 m/s. Assuming the (sub)giant star has  $1.1 M_{\odot}$ , the mass of the corresponding companion would be  $m_3 \sin i = 5.8 M_{\text{Jup}}$ , i.e., in the planetary or brown dwarf domain for most inclinations. However, the light curve modulations (both the large amplitude, the presence of only one minimum per period and no eclipses), allows us to discard this configuration.

A second (much more likely) scenario is that this short-period radial velocity modulation is a consequence of the high chromospheric activity of the G-type star. This interpretation is supported by the photometric observations, which present sinusoidal variability with approximately the same period - this photometric variability is generally accepted to be due to the presence of short-lived spots on the stellar surface which move with the giant's rotation period (Miszalski et al. 2013). Furthermore, the amplitude of these radial velocity variations, at roughly 1% of the rotation ve-



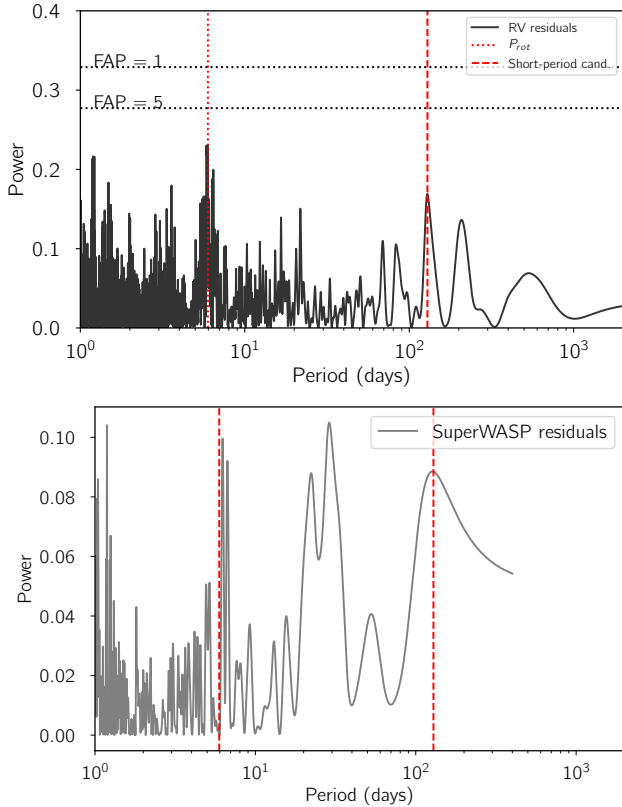


**Figure 9.** (Top:) Lomb-Scargle periodogram of the residuals of the radial velocity data after removing the long-period component. The false alarm probabilities (FAP) at 1% and 5% are marked with dotted lines. (Bottom:) Lomb-Scargle periodogram of the SuperWASP dataset after removing the 5.9 days period component. The peak at 129 days is displayed in red dashed line.

locity, is also consistent with amplitude of the photometric observations, at 1–2% depending on the filter. As such, this is the first time that the chromospheric activity of this star has been shown spectroscopically, principally due to the extremely high precision and good time coverage of the HERMES data.

### 3.4.3 The $\sim 129$ days period

By inspecting the periodogram of the residuals of the radial velocity after removing the long-period signal (Figure. 9), the second highest peak is found at  $\sim 129$  days. Despite not being statistically significant (false alarm probability larger than 5%), we remark this peak because we also found relevant modulation with the exact same periodicity in the photometric data (see Sect. 3.3 above).

We tried to fit the residuals with another Keplerian model, now assuming circular orbit for the sake of simplicity of the adopted model. Assuming that the 5.9 days variation in radial velocity is due to the stellar activity observed in the light curves, we can include in our model a Gaussian Process (GP) with a quasi-periodic kernel (see Faria et al. 2016) to account for the correlated noise introduced by the stellar activity mentioned before. The hyper-parameters of this model include an amplitude of the variations ( $\eta_1$ ), a correlation de-

correlation timescale ( $\eta_2$ ), and a periodic component with period  $\eta_3$ . The last hyper-parameter ( $\eta_4$ ) controls the weight of the two periodic components. The Keplerian model includes a residual systemic velocity of the system ( $V_{\text{sys},3}$ ), the semi-amplitude of the radial velocity signal ( $K_3$ ), the period of the additional component ( $P_3$ ), and its time of conjunction ( $T_{0,3}$ ). Added to these eight parameters, we also include a jitter parameter to account for possible white noise ( $\sigma_{\text{jit}}$ ). We provide uninformative priors for all of the parameters but restricting their ranges to particular regimes. In Table A1, we provide the priors.

The parameter space is explored by using the same approach explained in Sect. 3.4.1. Despite the uninformative priors, the MCMC chains converge into a solution corresponding to the periodicity found in the periodogram and in the superWASP light curve analysis. The median values for each parameter and their 68.7% confidence interval are provided in Table 4. The radial velocity semi-amplitude parameter is, however, not constrained, and we can only provide an upper limit of  $K_3 < 390$  m/s. Again assuming a  $1.1M_{\odot}$  for the primary star, this would imply a maximum projected mass of  $m_3 \sin i < 10.3 M_{\text{Jup}}$ , providing an absolute mass in the case of coplanarity with the PN waist of  $m_3 \sim 35.3 M_{\text{Jup}}$ . However, it is again really difficult to explain this peak in the light curve with such a low mass.

We have also explored the possibility of an eccentric orbit. In this case, we also obtain a median model in agreement with the  $\sim 129$ -days period. Interestingly, in this case, the posterior distribution of the eccentricity is very broad but favouring very high eccentricities ( $e > 0.5$ ), with the most probable value being around  $e \sim 0.75$ . We note that given the small amplitude of the signal and the rapid rotation of the star, the detection is somehow marginal but provides hints for the presence of a third guest in a highly eccentric orbit. This high eccentricity could be explained by the presence of the exterior massive companion (also in an eccentric orbit). Additionally, assuming  $e = 0.75$ , this third guest would be as close to the primary G-type star as  $r = 0.12$  AU during the periastron passage. This could thus be the source of the variability that we detected in the superWASP light curve with the same periodicity. However, with the current data we are not able to discuss the origin of the light curve modulations (i.e., irradiation or tidal interactions).

### 3.5 The puzzling $H\alpha$ double-peaked profile

Figure 10 shows the rapid variations of the  $H\alpha$  profile during the ELODIE (top panel), HERMES (middle, in a small sample) and CAFE (bottom) observations. The three datasets show clear  $H\alpha$  double-peaked profile that varies with very short time scales, with a strong absorption feature which reaches below the continuum level in some cases. Such  $H\alpha$  double-peaked profile is not new in LoTr 5 and was already reported by Jasniewicz et al. (1994) and Strassmeier et al. (1997). It has also been seen in other systems like, e.g., LoTr 1 (Tyndall et al. 2013) and Abell 35 (Acker & Jasniewicz 1990; Jasniewicz et al. 1992) although the origin is still unknown. Several explanations have been proposed, specially the chromospheric activity of the G-type star, the presence of an accretion disc or the existence of strong stellar winds. In the following, we will discuss these three possibilities in more detail.



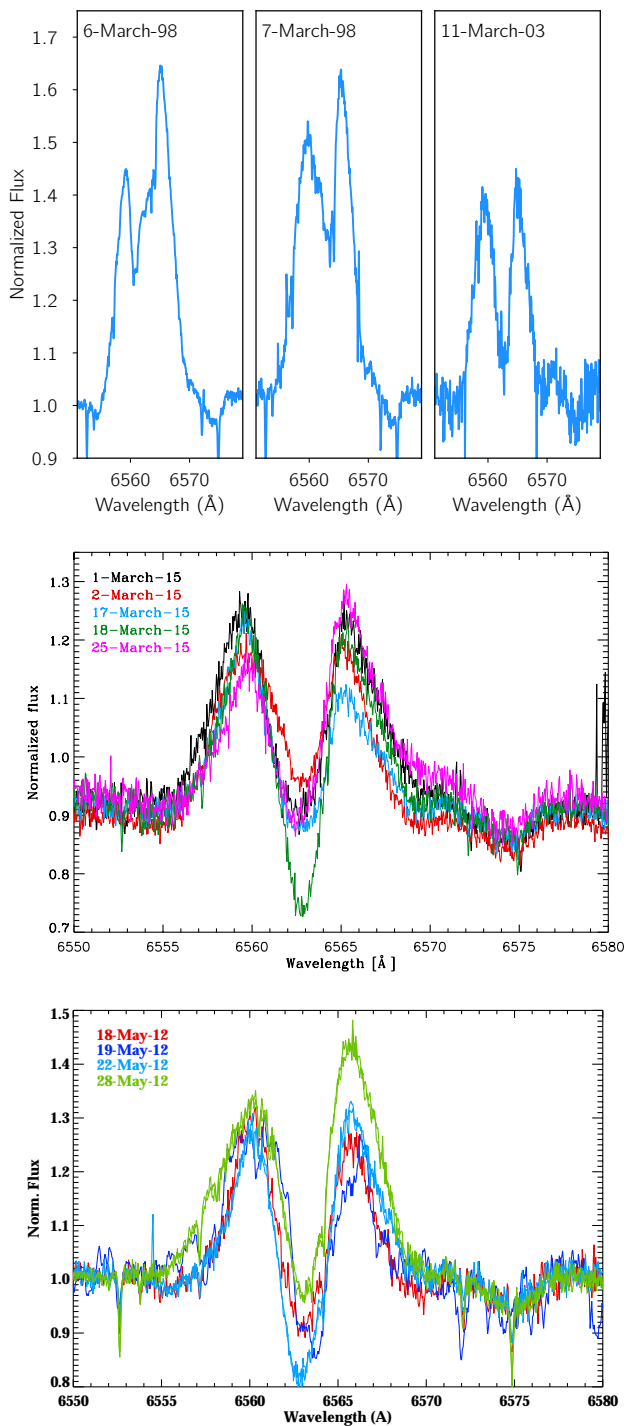


**Figure 10.** Variations in the  $H\alpha$  profile during the ELODIE (top panel), HERMES (middle panel) and CAFE observations (bottom panel).

### 3.5.1 Chromospheric activity

There is no doubt that the G-type star of HD 112313 has a high chromospheric activity. This is clearly indicated by the active-chromosphere indicators present in the spectrum. Strassmeier et al. (1997) already showed some of these relevant indicators like the emission in the Ca II H&K lines,

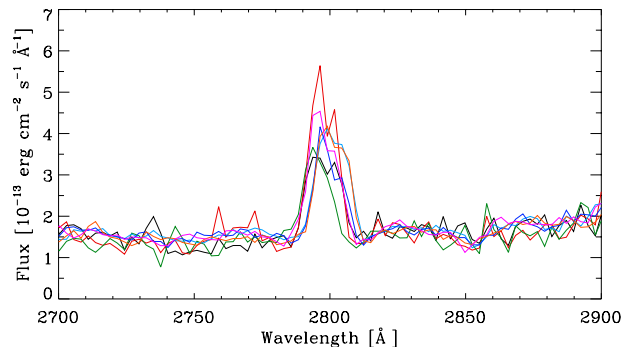


**Figure 11.** Variations in the Mg II  $\lambda 2800$  emission line in several IUE spectra.

the infrared triplet lines of Ca II  $\lambda 8498, 8542, 8662$  and the already mentioned broad, double-peaked  $H\alpha$  profile. Also, the Mg II h&k  $\lambda 2796, 2803$  lines appear in emission in the IUE spectra, as firstly shown by Feibelman & Kaler (1983). For the first time, we find fast variations of this line in the IUE spectra (see Figure 11), in contrast to what Jasniewicz et al. (1996) reported. Finally, it should not be forgotten the detection of X-rays emission in LoTr 5 (Apparao et al. 1992; Montez et al. 2010). According to Montez et al. (2010) the most likely explanation for this X-rays detection is the presence of coronal activity associated to the G star. All of these pieces seem to indicate that chromospheric activity plays an important role in LoTr 5. However, some features of the  $H\alpha$  profile remain unexplained. The most relevant is the full width at half maximum (FWHM) of the line, that is too high ( $450 \text{ km s}^{-1}$ ) to be due only to chromospheric activity. Also, if we measure the equivalent width (EW) of the  $H\alpha$  core emission (determined by subtracting an inactive star with the same effective temperature and surface gravity) it appears to be quite higher than that expected in the (sub)giant regime, according to Figure 5c in Strassmeier et al. (1990). In contrast, the EW is similar to that measured in FK Com, another rapidly rotating giant star that is known to have high chromospheric activity. FK Com presents an  $H\alpha$  double-peaked profile similar than HD 112313 (see, for instance, Kjurkchieva & Marchev 2005). However, we note that, in contrast to what occurs in FK Com, in LoTr 5 (i) there is no evidence of an accretion disc via RLOF (see 3.5.2) and (ii) there is not any phase dependency in the variation of the  $H\alpha$  profile (see below). All this would point out that part of the  $H\alpha$  line is not due to chromospheric activity.

Following the procedure explained in Acker & Jasniewicz (1990) for Abell 35, we have tried to find a modulation of the  $H\alpha$  profile with the rotation phase, by measuring the flux variation between the nearby continuum and the deepest point of the  $H\alpha$  absorption core. In contrast to the results found by Acker & Jasniewicz (1990) in the case of Abell 35, we do not find any correlation with the rotational period during the long time span of the observations in LoTr 5. We have inspected the  $H\alpha$  profile in all the Hermes spectra and we found no correlation with the rotation period, see Fig. A1, where we show the phased-folded trailed spectra of the  $H\alpha$  line with the rotation period.

The Ca II H&K  $\lambda 3933, 3967$  lines appear in emission in

the HERMES dataset (as already reported by [Strassmeier et al. 1997](#)). We do not find variations in these lines at the level of the H $\alpha$  variations that we find in HERMES data. Hence, Ca II H&K lines are not useful for studying the activity of the star.

### 3.5.2 Accretion disc around the possible close companion

The presence of an accretion disc in LoTr 5 has been also discussed in the literature. If indeed the H $\alpha$  emission was due to an accretion disk, then the double-peaked profile would come from two different emission regions instead of a broad emission feature. [Montez et al. \(2010\)](#) already discussed the system within this scenario: since the presence of an accretion disc would imply the Roche lobe overflow (RLOF), they calculated the Roche lobe radius ( $R_L$ ) assuming the synchronization of the rotation and orbital period (i.e., they assumed a close  $0.6M_{\odot}$  companion at  $\sim 5.9$  days). Under this configuration, the  $R_L$  was below the radius of the star, filling its Roche Lobe and allowing the existence of an accretion disc. However, from our radial velocity analysis, we know that it is not possible to have such a massive companion so close of the G-type star. On the contrary, in the case we would have a low-mass object at  $\sim 5.9$  days, the  $R_L$  would be  $\sim 16R_{\odot}$ , and the star could not have filled its Roche lobe. Therefore, with the current data, we conclude that it is not possible to have an accretion disc via RLOF in LoTr 5.

Finally, and as mentioned in Section 3.2, no significant infrared excess is identified in the SED, which would point out that an accretion disc is highly unlikely in the system.

### 3.5.3 The possible resemblance with symbiotic stars

Finally, it is worth mentioning that this double-peaked H $\alpha$  emission resembles the observed in some symbiotic stars (SS), the widest interacting binary systems known with a white dwarf accreting material from a giant star via stellar winds (see, e.g., [Van Winckel et al. 1993](#); [Burmeister & Leedj arv 2009](#)). These systems are sometimes embedded into a bipolar nebula similar to some PNe (like LoTr 5). However, apart from the complex H $\alpha$  profile, we do not find evidence of P-cygni profiles and/or strong complex emissions in any of the lines in the spectra of HD 112313. The only detection of P-cygni profiles in HD 112313 was reported by [Modigliani et al. \(1993\)](#), who found those profiles in the O V  $\lambda 1371$  and C IV  $\lambda 1548, 1550$  lines in the IUE spectra. From the analysis of these profiles, they concluded a fast wind speed of  $3300 \text{ km s}^{-1}$  (although we note that, if true, this fast wind more likely would come from the hot central star and not from the cool giant). In any case, we have re-analyzed the IUE spectrum used by [Modigliani et al. \(1993\)](#) for HD 112313 (SWP19909), as well as the rest of them -both in low- and high-resolution- and have not found any evidence of P-cygni profiles. All these spectra were extracted from the INES database; in order to double check the results, we have also retrieved the IUE spectra available from MAST<sup>9</sup>, that are reduced in an independent way to that of the INES archive. No P-cygni profiles are identified in MAST spectra either. The absence of these characteristic profiles and other prominent

features typical in symbiotic stars make it highly improbable that LoTr 5 belongs to this group.

With a high-quality spectrum of the nebula we would be able to place LoTr 5 in a diagnostic diagram (like those shown in [Ilkiewicz & Mikolajewska 2017](#)) to distinguish between symbiotic stars and planetary nebulae. Unfortunately, only a very weak H $\alpha$  flux (by [Frew et al. 2016](#)) and [O III]  $\lambda 4959, 5007$  (measured by [Kaler et al. 1990](#)) are published in the literature.

## 4 CONCLUSIONS AND DISCUSSION

We revisit the complex LoTr 5 system and discuss the still open questions around this object by means of radial velocity and archival (SuperWASP, ASAS and OMC) light curve analysis. For the first time, and based on both archive and new radial velocity data, we recover two orbital cycles of the long-period binary central star, confirming the orbital period of  $2689 \pm 52$  days with an eccentricity of  $0.249 \pm 0.018$ . After removing this long-period component from the radial velocity, the residual periodogram shows two interesting (although still not statistically significant) peaks: the first one, at  $\sim 5.9$  days, is also identified in the SuperWASP and ASAS periodograms. This periodicity was already known and is assumed to be the rotation period of the G-type subgiant; the second peak, at  $\sim 129$  days, albeit with low S/N, is also found when subtracting the 5.9 days component from the SuperWASP data (the most precise light curve we have). We analyze the  $\sim 129$  days periodicity and found that it could be compatible with a low-mass object (in the planetary or brown dwarf domain) with a high eccentricity. However, the current data are not enough to confirm such a third guest in the system and more dedicated data are mandatory to prove this scenario.

The possibility of a triple system is also discussed under other configuration: assuming a third object with the same orbital period as the rotation period (5.9 days), i.e., assuming synchronization of the rotation period of the G-type star and the orbital period of a possible close binary. However, it appears unlikely with the current data since the most plausible explanation for the 5.9-days periodicity found in the radial velocity and photometric data is, indeed, the activity of the G-type star.

Finally, and regarding the chromospheric activity, we also discuss the double-peaked H $\alpha$  profile seen in the spectra, which shows moderate variations in very short time span. It is clear that the G-type stellar component of HD 112313 has a high chromospheric activity. This is confirmed by the active-chromosphere indicators present in the UV and optical spectra, like the emission in the Ca II H&K lines, the infrared triplet lines of Ca II  $\lambda 8498, 8542, 8662$ , that appear less deep than in a non-active G-star with the same effective temperature and surface gravity (i.e., an emission component is clearly contributing to these absorption lines), as well as the Mg II h&k  $\lambda 2796, 2803$  lines, that appear in emission in the IUE spectra and show clear variations in intensity. However, some features of the complex H $\alpha$  profile appear not compatible with chromospheric activity (the most relevant is the high FWHM of the line), pointing out that at least part of the line is not due to chromospheric activity, and suggesting other possible explanations like the presence

<sup>9</sup> <https://archive.stsci.edu/iue/search.php>

of an accretion disk and/or stellar winds. Based on the calculation of the Roche lobe radius, we discard the presence of an accretion disk via Roche lobe overflow, since the star can not have filled its Roche lobe. In addition, the absence of P-cygni profiles in the spectra of LoTr 5 points out that stellar winds do not play an important role in this system and, therefore, that we are not dealing with a symbiotic star.

## ACKNOWLEDGEMENTS

We thank our anonymous referee for his/her comments that have improved the discussion of the data. A.A. acknowledges support from FONDECYT through postdoctoral grant 3160364. LFM acknowledges partial support from Spanish MINECO grant AYA2014-57369-C3-3-P (co-funded by FEDER funds). Based on observations obtained with the HERMES spectrograph, which is supported by the Research Foundation - Flanders (FWO), Belgium, the Research Council of KU Leuven, Belgium, the Fonds National de la Recherche Scientifique (F.R.S.-FNRS), Belgium, the Royal Observatory of Belgium, the Observatoire de Genève, Switzerland and the Thüringer Landessternwarte Tautenburg, Germany. Based on observations collected at the German-Spanish Astronomical Center, Calar Alto, jointly operated by the Max-Planck-Institut für Astronomie (Heidelberg) and the Instituto de Astrofísica de Andalucía (CSIC). Based on spectral data retrieved from the ELODIE archive at Observatoire de Haute-Provence (OHP). This publication makes use of VOSA, developed under the Spanish Virtual Observatory project supported from the Spanish MICINN through grant AyA2011-24052. Based on data from the OMC Archive at CAB (INTA-CSIC), pre-processed by ISDC. This paper makes use of data from the DR1 of the WASP data (Butters et al. 2010) as provided by the WASP consortium, and the computing and storage facilities at the CERIT Scientific Cloud, reg. no. CZ.1.05/3.2.00/08.0144 which is operated by Masaryk University, Czech Republic. This work used the python packages numpy, matplotlib, astroML, asciitable, pyTransit, kplr, and emcee.

## REFERENCES

- Aceituno J., et al., 2013, *A&A*, **552**, A31  
 Acker A., Jasniewicz G., 1990, *A&A*, **238**, 325  
 Acker A., Jasniewicz G., Gleizes F., 1985, *A&A*, **151**, L13  
 Alfonso-Garzón J., Domingo A., Mas-Hesse J. M., Giménez A., 2012, *A&A*, **548**, A79  
 Apparao K. M. V., Berthiaume G. D., Nousek J. A., 1992, *ApJ*, **397**, 534  
 Baranne A., et al., 1996, *A&AS*, **119**, 373  
 Bayo A., Rodrigo C., Barrado Y Navascués D., Solano E., Gutiérrez R., Morales-Calderón M., Allard F., 2008, *A&A*, **492**, 277  
 Bidelman W. P., Keenan P. C., 1951, *ApJ*, **114**, 473  
 Blanco-Cuaresma S., Soubiran C., Heiter U., Jofré P., 2014, *A&A*, **569**, A111  
 Boffin H. M. J., Jorissen A., 1988, *A&A*, **205**, 155  
 Bond H. E., Livio M., 1990, *ApJ*, **355**, 568  
 Bond H. E., Ciardullo R., Meakes M. G., 1993, in Weinberger R., Acker A., eds, IAU Symposium Vol. 155, Planetary Nebulae. p. 397  
 Burmeister M., Leedjävär L., 2009, *A&A*, **504**, 171  
 Ciardullo R., Bond H. E., Sipior M. S., Fullton L. K., Zhang C.-Y., Schaefer K. G., 1999, *AJ*, **118**, 488  
 Faria J. P., Haywood R. D., Brewer B. J., Figueira P., Oshagh M., Santerne A., Santos N. C., 2016, *A&A*, **588**, A31  
 Feibelman W. A., Kaler J. B., 1983, *ApJ*, **269**, 592  
 Foreman-Mackey D., Hogg D. W., Lang D., Goodman J., 2013, *PASP*, **125**, 306  
 Frew D. J., 2008, PhD thesis, Department of Physics, Macquarie University, NSW 2109, Australia  
 Frew D. J., Parker Q. A., Bojčić I. S., 2016, *MNRAS*, **455**, 1459  
 Graham M. F., Meaburn J., López J. A., Harman D. J., Holloway A. J., 2004, *MNRAS*, **347**, 1370  
 Gray D. F., 2005, The Observation and Analysis of Stellar Photospheres  
 Gray R. O., Corbally C. J., 1994, *AJ*, **107**, 742  
 Grevesse N., Asplund M., Sauval A. J., 2007, *Space Sci. Rev.*, **130**, 105  
 Gustafsson B., Edvardsson B., Eriksson K., Jørgensen U. G., Nordlund Å., Plez B., 2008, *A&A*, **486**, 951  
 Heber U., 2016, *PASP*, **128**, 082001  
 Ilkiewicz K., Mikolajewska J., 2017, preprint, ([arXiv:1708.05224](https://arxiv.org/abs/1708.05224))  
 Jasniewicz G., Acker A., Duquennoy A., 1987, *A&A*, **180**, 145  
 Jasniewicz G., Acker A., Freire Ferrero R., Burnet M., 1992, *A&A*, **261**, 314  
 Jasniewicz G., Acker A., Maun N., Duquennoy A., Cuypers J., 1994, *A&A*, **286**, 211  
 Jasniewicz G., Thevenin F., Monier R., Skiff B. A., 1996, *A&A*, **307**, 200  
 Jeffries R. D., Stevens I. R., 1996, *MNRAS*, **279**, 180  
 Jones D., Boffin H. M. J., 2017, *Nature Astronomy*, **1**, 0117  
 Jones D., Van Winckel H., Aller A., Exter K., De Marco O., 2017, preprint, ([arXiv:1703.05096](https://arxiv.org/abs/1703.05096))  
 Kaler J. B., Shaw R. A., Kwitter K. B., 1990, *ApJ*, **359**, 392  
 Kjurkchieva D. P., Marchev D. V., 2005, *A&A*, **434**, 221  
 Kondo Y., Boggess A., Maran S. P., 1989, *ARA&A*, **27**, 397  
 Kuczawska E., Mikolajewski M., 1993, *Acta Astron.*, **43**, 445  
 Lillo-Box J., Barrado D., Santos N. C., Mancini L., Figueira P., Ciceri S., Henning T., 2015, *A&A*, **577**, A105  
 Longmore A. J., Tritton S. B., 1980, *MNRAS*, **193**, 521  
 Malasan H. L., Yamasaki A., Kondo M., 1991, *AJ*, **101**, 2131  
 Mas-Hesse J. M., et al., 2003, *A&A*, **411**, L261  
 Miszalski B., et al., 2013, *MNRAS*, **436**, 3068  
 Modigliani A., Patriarchi P., Perinotto M., 1993, *ApJ*, **415**, 258  
 Montez Jr. R., De Marco O., Kastner J. H., Chu Y.-H., 2010, *ApJ*, **721**, 1820  
 Moultaqa J., Ilovaisky S. A., Prugniel P., Soubiran C., 2004, *PASP*, **116**, 693  
 Noskova R. I., 1989, *Pisma v Astronomicheskii Zhurnal*, **15**, 346  
 Pojmanski G., 1997, *Acta Astron.*, **47**, 467  
 Pollacco D. L., et al., 2006, *PASP*, **118**, 1407  
 Raskin G., et al., 2011, *A&A*, **526**, A69  
 Santerne A., et al., 2012, *A&A*, **544**, L12  
 Schnell A., Purgathofer A., 1983, *A&A*, **127**, L5  
 Strassmeier K. G., Fekel F. C., Bopp B. W., Dempsey R. C., Henry G. W., 1990, *ApJS*, **72**, 191  
 Strassmeier K. G., Hubl B., Rice J. B., 1997, *A&A*, **322**, 511  
 Thevenin F., Jasniewicz G., 1997, *A&A*, **320**, 913  
 Tyndall A. A., et al., 2013, *MNRAS*, **436**, 2082  
 Van Winckel H., Duerbeck H. W., Schwarz H. E., 1993, *A&AS*, **102**, 401  
 Van Winckel H., Jorissen A., Exter K., Raskin G., Prins S., Perez Padilla J., Merges F., Pessemer W., 2014, *A&A*, **563**, L10

**Table A1.** Priors adopted for the analysis of the different radial velocity components and scenarios.  $\mathcal{U}(a, b)$  stands for a uniform prior between a and b;  $\mathcal{G}(\mu, \sigma)$  are Gaussian priors with a mean  $\mu$  and standard deviations  $\sigma$ ; and  $\mathcal{MJ}(a, b)$  is a Modified Jeffries prior with a and b parameters.

Parameter	Long-period	5.95d	~129d (circ)	~129d (ecc)
$V_{\text{sys}}$ (km/s)	$\mathcal{U}(-30, 30)$	-	$\mathcal{U}(-10, 10)$	$\mathcal{U}(-10, 10)$
$P$ (days)	$\mathcal{U}(2000, 4000)$	X	$\mathcal{U}(115, 140)$	$\mathcal{U}(115, 140)$
$T_0$ (days)	$\mathcal{U}(2455000, 2459000)$	-	-	$\mathcal{U}(2454950, 2455080)$
$K$ (km/s)	$\mathcal{MJ}(0.005, 15)$	X	$\mathcal{MJ}(0.005, 15)$	$\mathcal{MJ}(0.005, 3)$
$e$	$\mathcal{U}(0, 1)$	-	-	$\mathcal{U}(0, 1)$
$\omega$ ( $^\circ$ )	$\mathcal{U}(0, 360)$	-	-	$\mathcal{U}(0, 360)$
$\eta_1$ (dex)	-	-	$\mathcal{U}(-10.6, -6.9)$	$\mathcal{U}(-10.6, -6.9)$
$\eta_2$ (days)	-	-	$\mathcal{U}(6, 200)$	$\mathcal{U}(6, 200)$
$\eta_3$ (days)	-	-	$\mathcal{G}(5.95, 0.1)$	$\mathcal{G}(5.95, 0.1)$
$\eta_4$	-	-	$\mathcal{U}(-10, 20)$	$\mathcal{U}(-10, 20)$

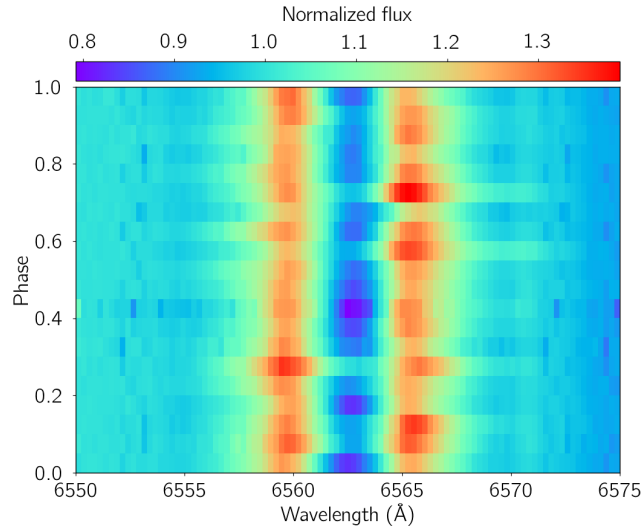


**Figure A1.** Phase-folded trailed spectra of the  $H\alpha$  line with the rotation period ( $\sim 5.9$  days) of the G-type star. No correlation is identified with such period, pointing out variations in the double-peaked  $H\alpha$  profile are not only consequence of the chromospheric activity of the G-type star.

## APPENDIX A:

This paper has been typeset from a  $\text{\TeX}/\text{\LaTeX}$  file prepared by the author.